Electrons in cold water clusters: An ab initio molecular dynamics study of localization and metastable states

Ondrej Marsalek,[a] Frank Uhlig,[b] and Pavel Jungwirth[a*]

[a]*Institute of Organic Chemistry and Biochemistry, Academy of Sciences of the Czech Republic and Center for Biomolecules and Complex Molecular Systems, Flemingovo nám. 2, 16610 Prague 6, Czech Republic,* [b]*Wilhelm-Ostwald-Institut für Physikalische und Theoretische Chemie, Linnéstrasse 2, 04103 Leipzig, Germany.*

*Corresponding author: pavel.jungwirth@uochb.cas.cz

Abstract

Ab initio molecular dynamics simulations were performed with the aim to follow two scenarios for an excess electron in cold water clusters. In the first one, an electron is attached to a quenched neutral cluster. Such an electron, initially very delocalized and loosely bound, shrinks somewhat and increases its vertical detachment energy to 1 – 1.5 eV within several picoseconds. Unlike in warm liquid clusters, the electron in this cold system does not, however, reach a more compact and strongly bound structure. In contrast, if an equilibrated negatively charged water cluster with a well localized excess electron is instantaneously quenched to ~0 K, the electron remains strongly bound in a water cavity and practically does not change its size and binding energy. These results have important consequences for detailed interpretation of photoelectron spectroscopy measurements of electrons solvated in aqueous clusters and liquid water microjets.

Introduction

One of the pressing questions concerning the structure and dynamics of a hydrated electron[1-5] concerns the relation of its properties in water clusters and in the liquid bulk. This question is not only how clusters of increasing size approach the bulk limit but also how different the experimental conditions in the two situations are.[6-12] A crucial property of a solvated electron is its vertical binding energy, i.e., the negative of the vertical detachment energy (VDE) of the anionic system. Its importance is also reflected in the fact that experiments on negatively charged water clusters[6,8,12] have been used to extrapolate its value to the bulk limit, which has been hard to obtain directly. Most recently, direct VDE measurements in the aqueous bulk have become feasible thanks to the technique of liquid microjets.[13-15] In this context it is imperative to properly establish the relation between cluster and microjet experiments. While the former systems are solid, having effective temperatures below 150 K,[12] the latter are liquid with temperatures above the freezing point.[13,15]

A typical feature of the experiments on negatively charged water clusters is that several isomers with distinct VDEs are observed for a given system size.[8,12] Depending on the particular way of cluster preparation these isomers are populated with varying abundances.[12] There is ongoing discussion about the structural interpretation in terms of either the position (surface vs interior) or different surface states of the electron.[8,12,16-21] Attempts have also been made to extrapolate the VDEs of these isomers to infinite size and interpret the extrapolated values in terms of different structures (bulk vs surface) of an

electron solvated in liquid water.[8,12,13] There is, however, a potential problem with such interpretations. Namely, in the microjet experiment, equilibrium liquid state conditions can be assumed for the solvated electron.[13,15] However, the isomers observed in the solid clusters do not necessarily correspond to an equilibrium situation but can reflect metastable situations pertinent to their experimental preparation.[11,12,20,21] The issues to be addressed in such extrapolations are, therefore, connected not only with different temperatures and phases (liquid vs amorphous solid or crystalline) but also with thermodynamic vs kinetically trapped states.

Problems connected with the metastability of the cluster states of the solvated electron and the corresponding dependence of the result on the method of preparation have been addressed both in experiments[12] and in simulations.[20,21] Comparison between two experiments with different ways of formation and storing of the water cluster anions is revealing.[8,12] Some isomers are present in both measurements, while others show up only in one experiment, which again points to their metastable nature. Related calculations, treating the electron as a quantum particle and water molecules classically, confirm that the occurence and population of different isomers reflects the thermal history of the cluster.[20] Most recently, we have performed ab initio molecular dynamics simulations of the localization process following electron attachment to cold or warm neutral water clusters.[21] Using a density functional theory based all (valence) electron approach, we have shown that at 300 K the excess electron attached to a neutral water cluster relaxes to an equilibrium solvated state within 1.5 ps, while at 20 – 50 K it becomes trapped in a metastable state about half way between the initial and the fully relaxed state.[21] Here, we

employ similar computational techniques to investigate and analyze electrons in cold water clusters prepared in different ways. Out of the various possibilities,[20] we chose to compare two very different scenarios. In the first one, the electron attaches to a cold neutral cluster and localizes afterwards, while in the second one an equilibrated warm negatively charged water cluster is quenched to 0 K. This comparison allows us to characterize in detail the nature of electrons localized in or on cold water clusters prepared under different conditions.

Methods

We performed ab initio molecular dynamics (AIMD) simulations for anionic clusters consisting of 32 water molecules. Initial conditions for the trajectories were prepared in two different ways. In the first one, structures from an AIMD of a neutral water cluster were taken and energy minimized and, at t = 0, the number of electrons was increased by 1. Eight trajectories were launched from these initial geometries with velocities sampled from Maxwell-Boltzmann distributions at 30-50 K. In the second one, geometries were obtained by energy minimization of 47 structures obtained in previous AIMD simulations of $(H2O)_{32}^-$ at 300 K.[21] Subsequently, two of these were used as initial conditions for MD trajectories. Classical equations of motion for the nuclei were propagated with a timestep of 0.5 fs with no temperature coupling.

Energies and forces were evaluated using the Becke, Lee, Yang and Parr (BLYP) exchange-correlation functional.[22,23] Dispersion interactions were accounted for using empirical pairwise damped London terms.[24] It was shown previously that this combination provides a very good description of liquid water.[25] To correct for the self interaction error,

which is an important issue for open shell systems, the functional was augmented with an additional term depending on the electron density of the unpaired electron.[26,27] To this end, we worked within a restricted open shell formulation of the density functional theory. The Kohn-Sham orbitals were expanded into an atom-centered triple-zeta basis set with two polarization functions, optimized for condensed molecular systems,[28] in conjunction with an auxiliary plane wave basis with a cutoff of 280 Ry for the electronic density. The Goedecker-Teter-Hutter norm-conserving pseudopotentials[29] replaced the oxygen core electrons. The system was placed in a 20×20×20 $Å^3$ box and an open boundary conditions Poisson's solver,[30] appropriate for clusters, was employed. For a proper description of the diffuse part of the spin density an additional grid of 1000 Gaussian functions with width of 0.189 $Å^{-1}$ and spacing of 2 Å was placed within the box.[21] VDE was evaluated as the difference between ground state energies of the cluster before and after electron detachment, in the geometry of the anion. Calculations were performed using the Quickstep module of the freely available CP2K program package.[31]

Below, we provide for reference definitions of various quantities monitored during the AIMD runs. Due to the restricted open-shell formalism employed, the total spin density of the system coincides with the density of the singly occupied molecular orbital (SOMO):

$$s(\mathbf{r}) = \Phi_{SOMO}(\mathbf{r})\Phi^{*}_{SOMO}(\mathbf{r}).$$

The spin density itself is normalized as

$$\int s(\mathbf{r}) d^3 r = 1.$$

The two main observables monitored throughout all of the simulations are the first and second moments of the spin distribution. Whereas the first moment $\mathbf{r}_c$ provides the center of the spin distribution

$$\mathbf{r}_c = \int \mathbf{r} s(\mathbf{r}) d^3 r ,$$

the second moment corresponds to the gyration tensor

$$\mathbf{S} = \int (\mathbf{r} - \mathbf{r}_c)(\mathbf{r} - \mathbf{r}_c) s(\mathbf{r}) d^3 r .$$

This tensor has three eigenvalues, denoted as λ_x^2, λ_y^2 and λ_z^2. For a description of the size of the excess electron we use the radius of gyration $\mathbf{r}_g$ which can either be defined as

$$r_g = \sqrt{\int s(\mathbf{r})(\mathbf{r} - \mathbf{r}_c)^2 d^3 r}$$

or using the three eigenvalues of the gyration tensor

$$r_g = \sqrt{\left(\lambda_x^2 + \lambda_y^2 + \lambda_z^2\right)}.$$

The gyration tensor is symmetric and positive-definite, hence all its eigenvalues are positive as well. Thus, we can approximate the shape of the spin distribution as an ellipsoid with its half-axes equal to λ_x^{-1}, λ_y^{-1} and λ_z^{-1}. Several shape descriptors are available for such an ellipsoid.[32] The asphericity b determines the deviation from a perfect sphere,

$$b = \lambda_z^2 - \frac{1}{2}\left(\lambda_x^2 + \lambda_y^2\right).$$

It acquires non-negative values and it is zero for a perfect sphere. The deviation from cylindric symmetry (acylindricity) is

$$c = \left(\lambda_y^2 - \lambda_z^2\right),$$

which is also always non-negative and zero for cylindric symmetry. The relative shape anisotropy, given by:

$$\kappa^2 = \frac{b^2 + \frac{3}{4}c^2}{r_g^4}.$$

is an overall measure of the deviation from any kind of symmetry of the ellipsoid. It is bounded between zero and one, with zero corresponding to a perfect sphere.

Results and Discussion

In this study, we compare the behavior of the excess electron in cold water clusters prepared in two different ways: i) by attaching an electron to a neutral system which has been thermally equilibrated and then instantaneously quenched to 0 K or ii) by instantaneously cooling to 0 K a previously thermally equilibrated negatively charged cluster, with the electron occupying a well developed cavity and being strongly bound. In each case, we monitor the dynamics started from these initial conditions with the total energy of the system kept constant. Figures 1 and 2 show representative sets of snapshots from these trajectories (for animations of these trajectories see Supporting Information). We see that the two different ways of preparation of the cold clusters lead to qualitatively different structure and dynamics of the excess electron. When the electron is attached to a cold cluster (Figure 1), it is initially strongly delocalized over the cluster surface and within several picoseconds partially localizes at one side of the outer surface of the water clusters. As also discussed in previous studies,[21,33] this partial localization is due to a slight

reorganization of the dangling hydrogens of surface water molecules. However, in the cold water cluster there is not enough flexibility to allow for a creation of a polarized cavity, which would lead to a fully solvated electron. Such an equilibrated cavity electron forms in a warm cluster and remains largely intact upon cooling of this structure (Figure 2). Moreover, the shape of the excess electron prepared in this way mostly does not change during dynamics after cooling (Figure 2). It is worth mentioning at this point that the excess electron in the warm cluster, while strongly localized most of the time, can transiently acquire rather delocalized structures.[18] If such a structure is quenched to 30-50 K, we found that in the subsequent dynamics the electron remains delocalized at the cluster surface.

Time evolution of the radius of gyration of excess electrons prepared in the two ways described above is depicted in Figure 3. An electron attached to a quenched neutral water cluster starts gradually shrinking from its initial radius of more than 6 Å. However, on the timescale of the (several picosecond) simulations it remains significantly larger than an electron equilibrated at 300 K, with radius below 3 Å. In contrast, for an equilibrated negatively charged water cluster quenched to 0 K the already small electron further slightly shrinks and preserves its smaller size for the whole duration of the "cold" trajectory. The sizes of excess electrons prepared in these two ways thus appear on opposite tails of the equilibrium size distribution in the warm cluster (Figure 3). Figure 4 shows for the same set of trajectories as in Figure 3 the corresponding time evolution of VDE. For electrons attached to cold water clusters their vertical binding shifts from about -0.5 eV to -1 to -1.5 eV. These values are still rather far from the -2.5 to -3 eV binding of electrons in clusters equilibrated at 300 K, indicating that the clusters are kinetically trapped.[20,21] Note also that

cooling of an equilibrated negatively charged cluster leads to small increase of electron binding, which then remains roughly constant as time evolves (Figure 4).

Figure 5 shows the time evolution of the radius of gyration, VDE, and the distance between the center of the electron and center of mass of the cluster for a representative trajectory started by attaching an electron to an instantaneously quenched equilibrated neutral water cluster. As in our previous studies,[18,21] we see a very strong correlation between the size of the excess electron and its vertical binding energy. In contrast, there is little correlation between the VDE and the position of the electron with respect to the water cluster. This indicates that photoelectron spectroscopy is an excellent tool for distinguishing between delocalized and compact excess electron structures. However, it does not provide direct information about the position (interior vs interfacial) of the excess electron.

A direct presentation of the correlation between the radius of gyration and VDE of the excess electron is provided in Figure 6. We see that the two investigated ways of preparing cold excess electrons lead to filling separate regions of phase space. Electrons attached to equilibrated and then quenched clusters fill during subsequent dynamics a narrow region where the radius of gyration changes from 6.5 to 3 Å and, in concert, VDE moves from 0.5 to 2 eV. In contrast, when an equilibrated negatively charged water cluster is quenched to 0 K, the phase space region encompasses small radii of gyration (roughly 2 – 3 Å) and strong electron binding (about -2.5 to -4 eV) with zero overlap with the situation where the electron is attached to cold clusters (Figure 6). The phase space region

corresponding to equilibrated anion clusters at 300 K lies in-between these two sets, overlapping on one end with the quenched negatively charged clusters, while being separated by a gap from electrons attached to cold clusters (Figure 6). The latter confirms that attaching an electron to a cold cluster does not lead (at least on the timescale of the simulation) to an equilibrated strongly bound electron, but rather to a weak electron binding energy of a kinetically trapped species. Figure 7 shows similar correlations as in Figure 6, but now between the asymmetry parameter of the excess electron[27] and its radius of gyration or VDE. We see that the extended, loosely bound structures, pertinent to electron attachment to a cold cluster, start as rather asymmetric distributions, which become more symmetric as the electron (partially) localizes. The more compact and more strongly bound structures, corresponding to equilibrated negatively charged clusters, both before and after cooling, tend to be also more symmetric as seen from lower values of the asymmetry parameter.

The kinetic trapping of the structures obtained from dynamics started by electron attachment to neutral clusters quenched to 0 K is further demonstrated in Figure 8, which shows the time evolution of the root mean square deviation (RMSD) from the t = 0 structure as a function of time for a representative trajectory. We see an increase of the RMSD from 0 to about 1 Å within the first few picoseconds, which corresponds to small rearrangements of the surface water molecules as the electron starts to localize. However, the reorientation of water molecules then stops as exemplified by the leveling of the RMSD. In contrast, at ambient conditions RMSD continues to increase (Figure 8) as the cavity for the strongly bound electron forms in sufficiently large water clusters (such as that

investigated here) and moves by diffusion in the liquid cluster. This, however, does not happen in cold clusters and, consequently, the system becomes kinetically trapped. These observations have important implications concerning the validity of extrapolations of the properties of the excess electron from cold clusters to the bulk liquid. If experiments could be done for warm liquid clusters, such extrapolation would be well justified. However, since the kinetically trapped structures with weakly bound electrons tend to disappear upon heating, it is questionable whether such extrapolations to liquid water are justified. This in particular concerns the experimentally observed cold cluster isomers with less negative VDEs,[8,12] which do not seem to have an analogue in the ambient liquid.

Our results concerning the structure and dynamics of the excess electron are only as good as the underlying electronic structure description. It is, therefore, important to establish the reliability of the results with respect to the employed basis set and density functional method. The former issue is of particular importance for proper description of delocalized structures such as the excess electron. We found out that adding a regularly spaced grid of diffuse Gaussian functions is an effective and economic way of dealing with this problem. Figures 9 and 10 demonstrate the convergence of the crucial properties of the excess electron – its radius of gyration and VDE, with the number of Gaussian functions added. We see that for an excess electron in a well developed cavity convergence is achieved at around 500 basis functions. For a more diffuse structure of the excess electron convergence is, as expected, somewhat slower, nevertheless 1000 basis functions (which in the present setup corresponds to a grid spanning the whole box) provide practically converged radius of gyration and VDE. Figure 11 shows the effects of additional Gaussian

functions and the self-interaction correction[26,27] on the radius of gyration, position of the excess electron, and its VDE along a representative trajectory (same trajectory as in Figure 5; first 5 ps) corresponding to an electron attached to a quenched neutral cluster. We see that the effects of both the additional basis set and the self-interaction correction are important. Additional Gaussians allow accommodating better the excess electron, particularly in regions where no atoms of water molecules are present, which leads to its increase in size and distance from the center of cluster. At the same time a more complete basis set results in a more strongly bound excess electron.

Density functional methods within the generalized gradient approximation (such as BLYP) cannot provide an exact description of the excess electron.[34] They tend to overshoot the VDE of the excess electron, which may be partly due to an unbalanced description of system with varying number of electrons, i.e., before and after electron detachment. The self-interaction correction removes a significant part of the spurious self-repulsion of the excess electron. This allows the electron to better localize, leading to more compact and more strongly bound structures. Quantitatively, inclusion of the self-interaction correction increases the VDE by up to 0.5 eV. Since we do not correct for self-interaction error the closed shell state after ionization this increase may to some extent be artificial. Nevertheless, the structure and dynamics of the anionic clusters, which are in the focus of our study, should not be affected by this.

Conclusions

We performed ab initio molecular dynamics simulations of an excess electron in cold water clusters containing 32 water molecules, comparing two ways of preparation of the initial conditions of the system. Within the first scenario, we attached at t = 0 an excess electron to a neutral cluster, previously equilibrated (at 300 K) and then instantaneously quenched to 0 K. In the second approach, a negatively charged water cluster was first equilibrated at 300 K and then instantaneously quenched to 0 K, after which the dynamics was monitored. In the first case, the initially very delocalized and loosely bound electron partially relaxed, which is connected with a decrease of its size and increase of its vertical detachment energy from about 0.5 to 1 – 1.5 eV within several picoseconds. However, at these cryogenic conditions the excess electron in a sufficiently large water cluster, such as the one investigated here, does not reach equilibrium (at least not on the picosecond timescale), but rather becomes kinetically trapped. In the second scenario, the excess electron remains well localized in a water cavity. As a matter of fact, cooling of equilibrated negatively charged water clusters, possessing a well localized excess electron, even increases VDEs and decreases the electron size. The size and binding energy of such an excess electron change little during subsequent dynamics. Our results demonstrate, in agreement with previous studies,[12,20,21] that the properties of the excess electron in cryogenic water clusters depend on the details of the preparation of the system. This also raises questions concerning the validity of direct extrapolations of properties of electrons in cold water clusters to the bulk liquid.[13,21]

Acknowledgments

Support from the Czech Science Foundation (grants 203/08/0114) and the Czech Ministry of Education (grant LC512) is gratefully acknowledged. Part of the work in Prague was supported via Project Z40550506. OM acknowledges support from the International Max-Planck Research School for Dynamical Processes in Atoms, Molecules and Solids.

Figure captions:

Figure 1: Snapshots of the localization process following the attachment of an electron to a cold neutral water cluster. (a) The moment of electron attachment (t = 0 fs), (b) snapshot after partial localization on the surface (t = 1.75 ps), and (c) after further relaxation to a metastable state (t= 5 ps). Isovalues correspond to electron densities of 0.003, 0.0005, and 0.0002 au.

Figure 2: Snapshots from a run of an anionic water cluster equilibrated at 300 K and then instantaneously quenched to 0 K. (a) t = 0 fs and (b) after 5 ps molecular dynamics at constant energy.

Figure 3: Radius of gyration of the excess electron as a function of time for different types of trajectories. Runs started from quenched equilibrated anionic water clusters are shown in blue (2 trajectories), runs started by attachment of the electron to a quenched neutral water cluster are shown in other colors (8 trajectories). Equilibrium runs at T = 300 K are shown in gray for reference (6 trajectories).

Figure 4: Vertical detachment energy of the excess electron as a function of time for different types of trajectories. Runs started from quenched equilibrated anionic water clusters are shown in blue (2 trajectories), runs started by attachment of the electron to a quenched neutral water cluster are shown in other colors (8 trajectories). Equilibrium runs at T = 300 K are shown in gray for reference (6 trajectories).

Figure 5: Time evolution of the radius of gyration (top panel), vertical detachment energy (middle panel), and average distance of the excess electron from the cluster center of mass (bottom panel) for a representative trajectory corresponding to initial attachment of the electron to a quenched neutral water cluster.

Figure 6: Correlation between the vertical detachment energy and the radius of gyration of the excess electron for different types of trajectories and configurations. A set of geometries obtained by cooling equilibrated anionic water clusters is shown in black, runs started from three of those geometries are depicted in blue, runs started by attachment of an electron to a quenched neutral water cluster are shown in other colors (8 trajectories). For comparison, equilibrium runs at T = 300 K are shown in gray (25 ps total simulation time).

Figure 7: Correlation between shape anisotropy and radius of gyration (top panel) and vertical detachment energy (bottom panel) for different types of trajectories and configurations. A set of geometries obtained by cooling equilibrated anionic water clusters is shown in black, runs started from three of those geometries are depicted in blue, runs started by attachment of an electron to a quenched neutral water cluster are shown in other colors (8 trajectories). For comparison, equilibrium runs at T = 300 K are shown in gray (25 ps total simulation time).

Figure 8: Root mean square deviation of the system from its initial geometry as a function of time for a representative trajectory, where the excess electron has been attached to a quenched neutral cluster at t = 0 (dark blue). For comparison, results for three equilibrium runs at 300 K are shown in grey.

Figure 9: Radius of gyration (top panel) and vertical detachment energy (bottom panel) for a representative cluster geometry with the excess electron in a well developed cavity, as a function of the number of ghost atoms used as additional diffuse basis functions. A spherical cutoff from the center of the excess electron is used to decrease the number of ghost atoms.

Figure 10: Radius of gyration (top panel) and vertical detachment energy (bottom panel) for a representative cluster geometry with the excess electron in a diffuse surface state, as a function of the number of ghost atoms used as additional diffuse basis functions. A spherical cutoff from the center of the excess electron is used to decrease the number of ghost atoms.

Figure 11: Time evolution of the radius of gyration (top panel), vertical detachment energy (middle panel), and average distance of the excess electron from the cluster center of mass (bottom panel) for the same trajectory as in Figure 5 comparing calculations with self interaction correction and additional Gaussian basis functions (blue) to calculations lacking either the former (red) or the latter (green) item.

Figure 1

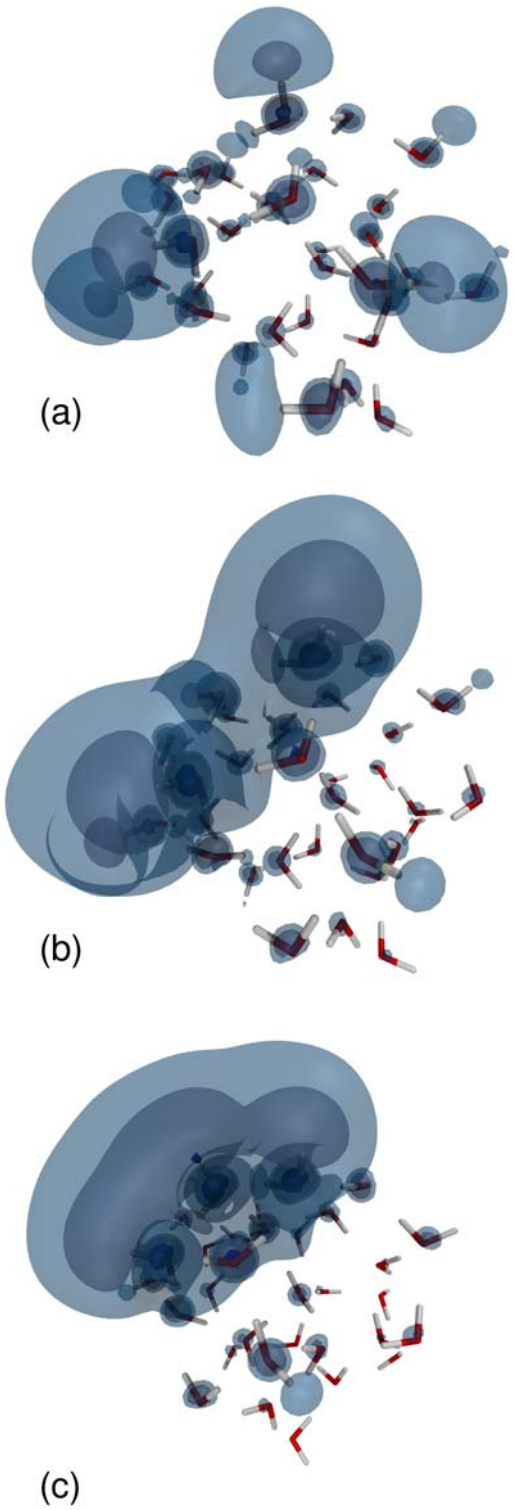

Figure 2

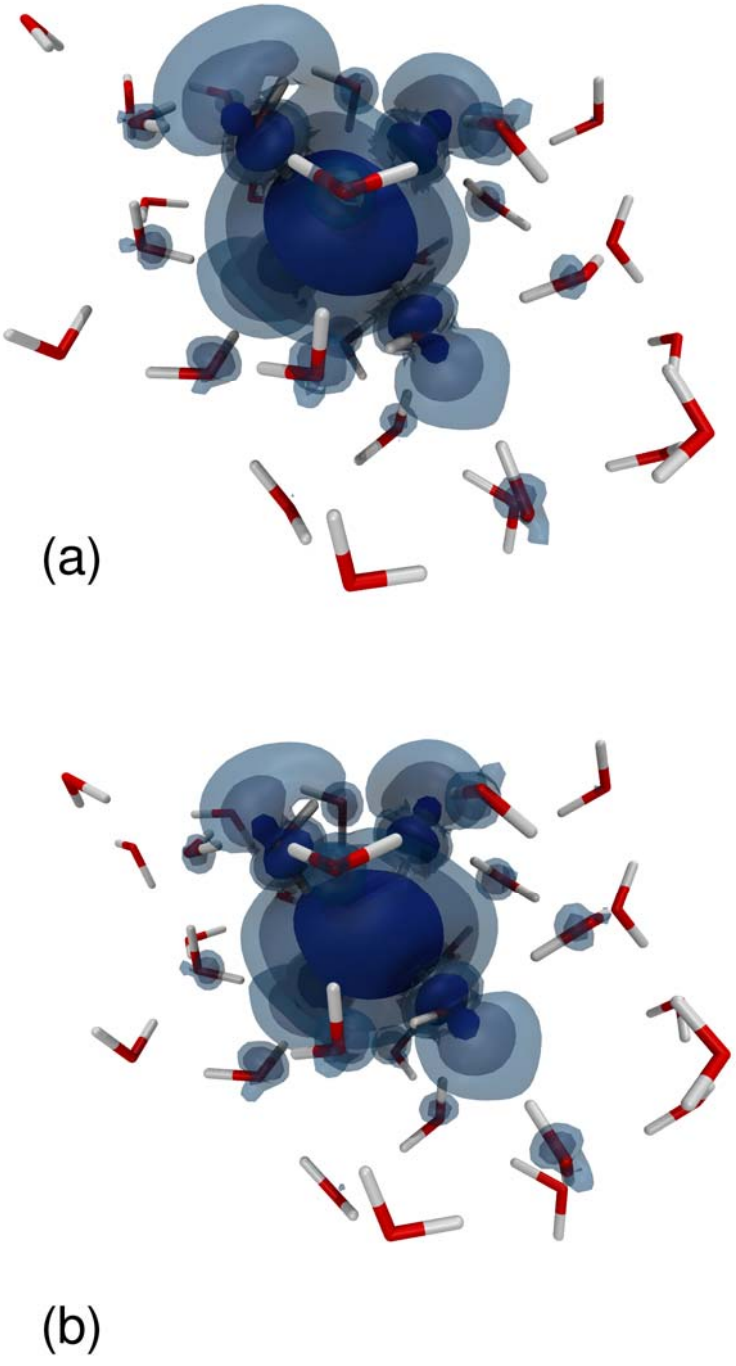

Figure 3

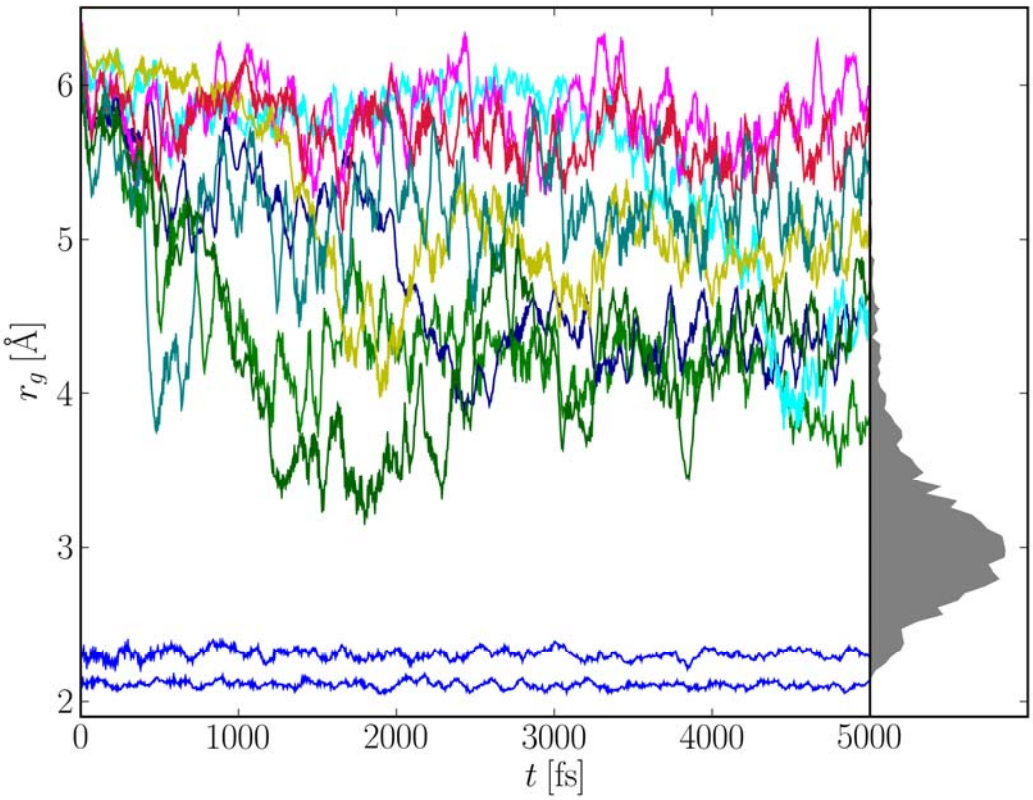

Figure 4

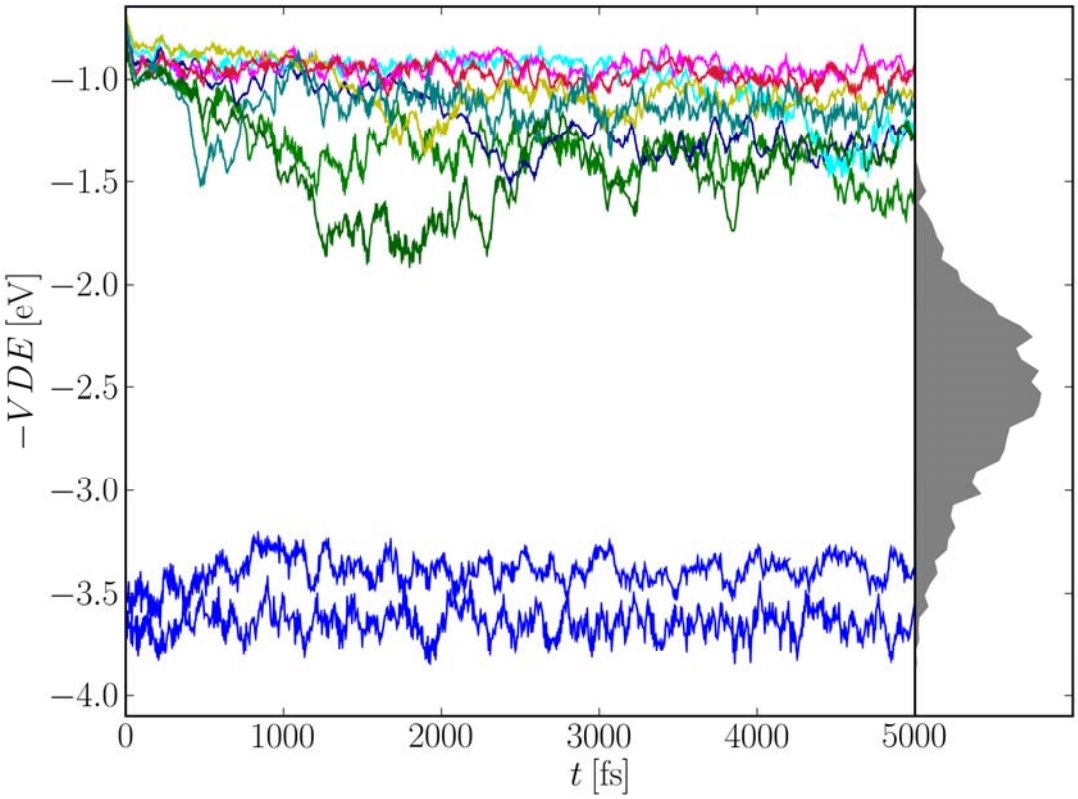

Figure 5

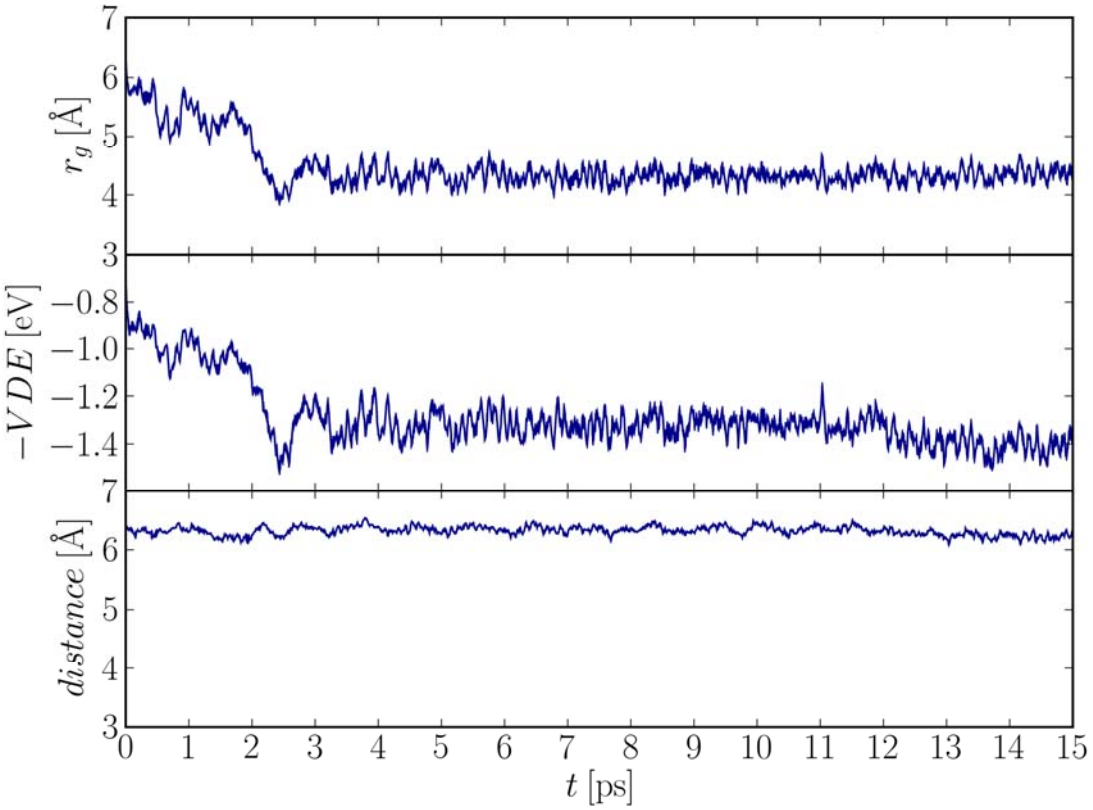

Figure 6

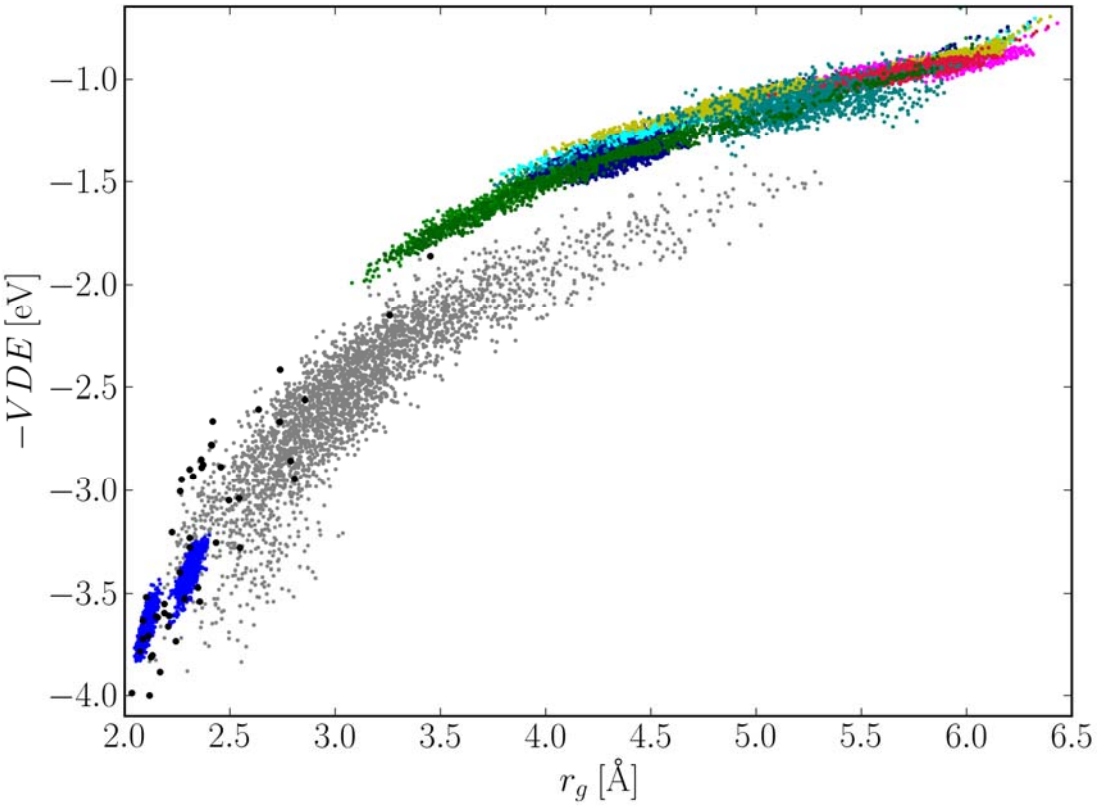

Figure 7

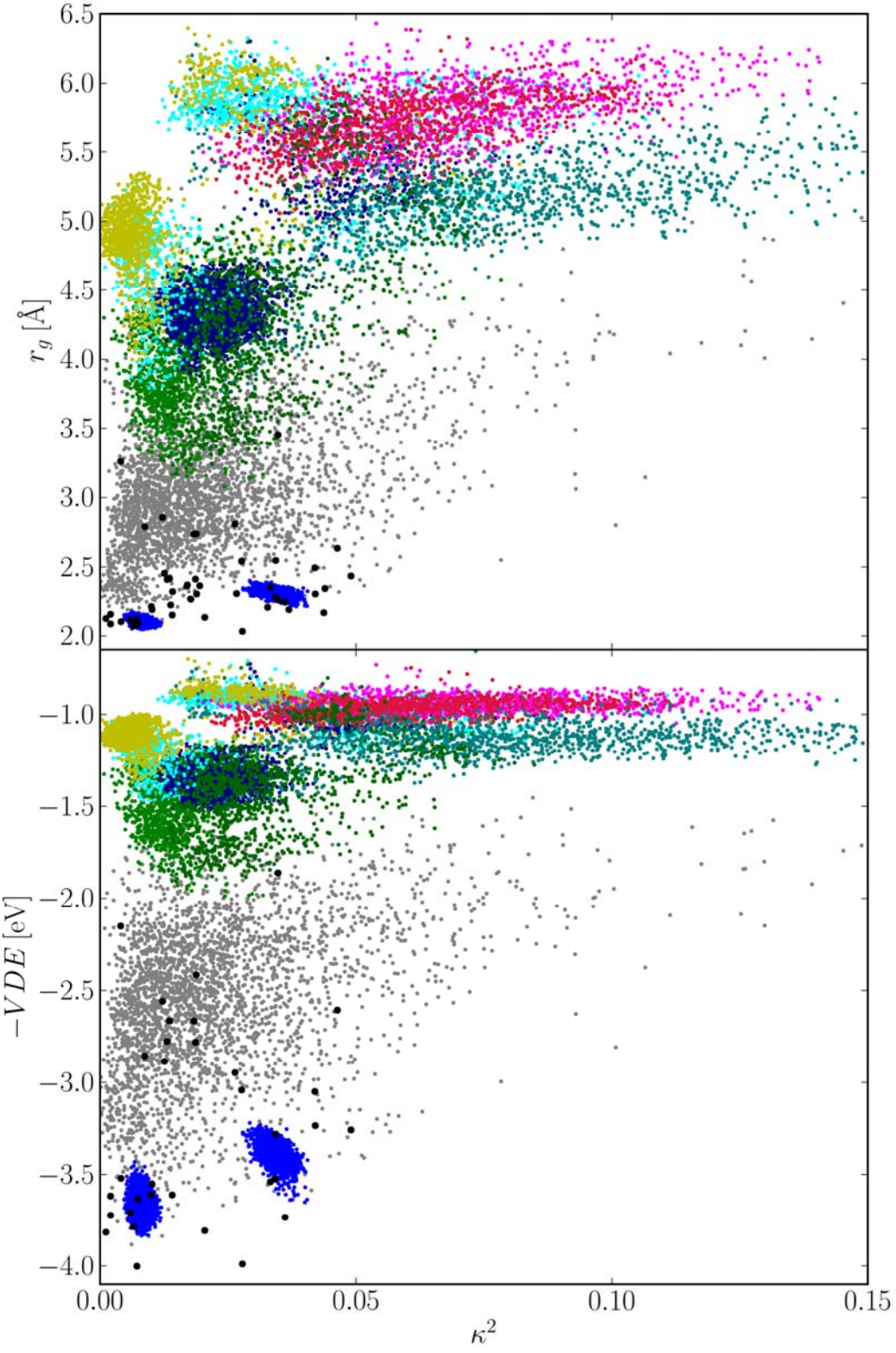
6.5
6.0
5.5
5.0
4.5
4.0
3.5
3.0
2.5
2.0
r_g [Å]
−1.0
−1.5
−2.0
−2.5
−3.0
−3.5
−4.0
$-VDE$ [eV]
0.00
0.05
0.10
0.15
κ^2

Figure 8

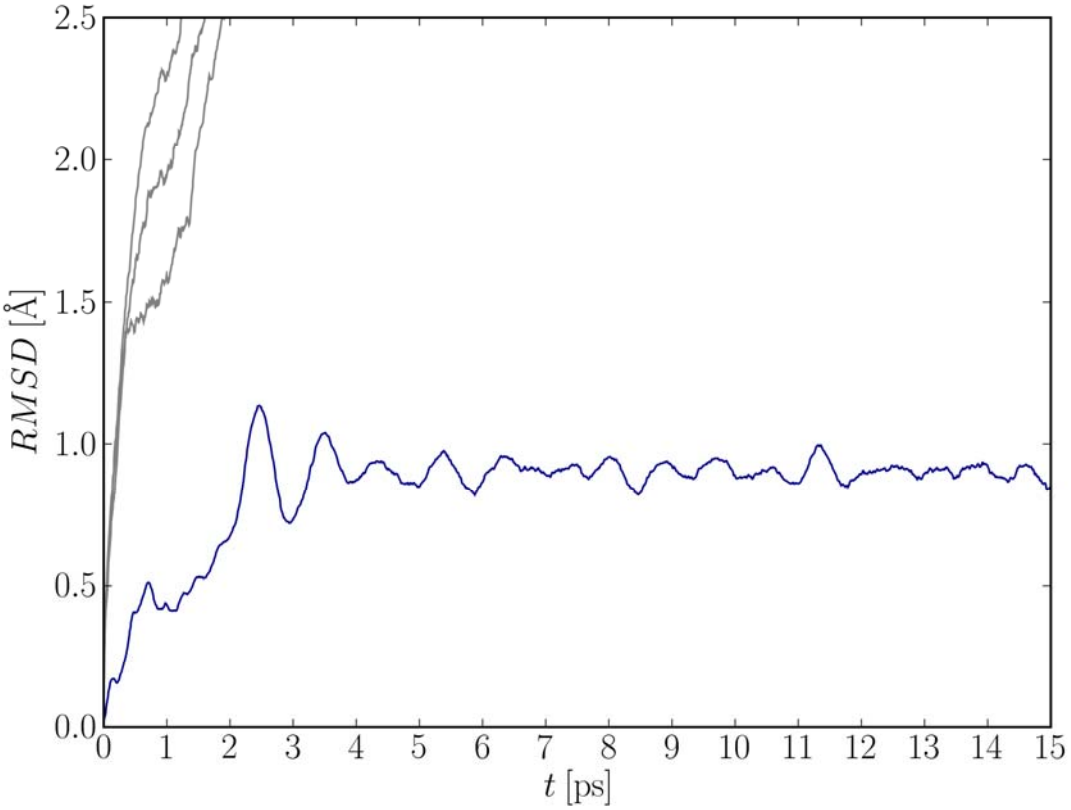

Figure 9

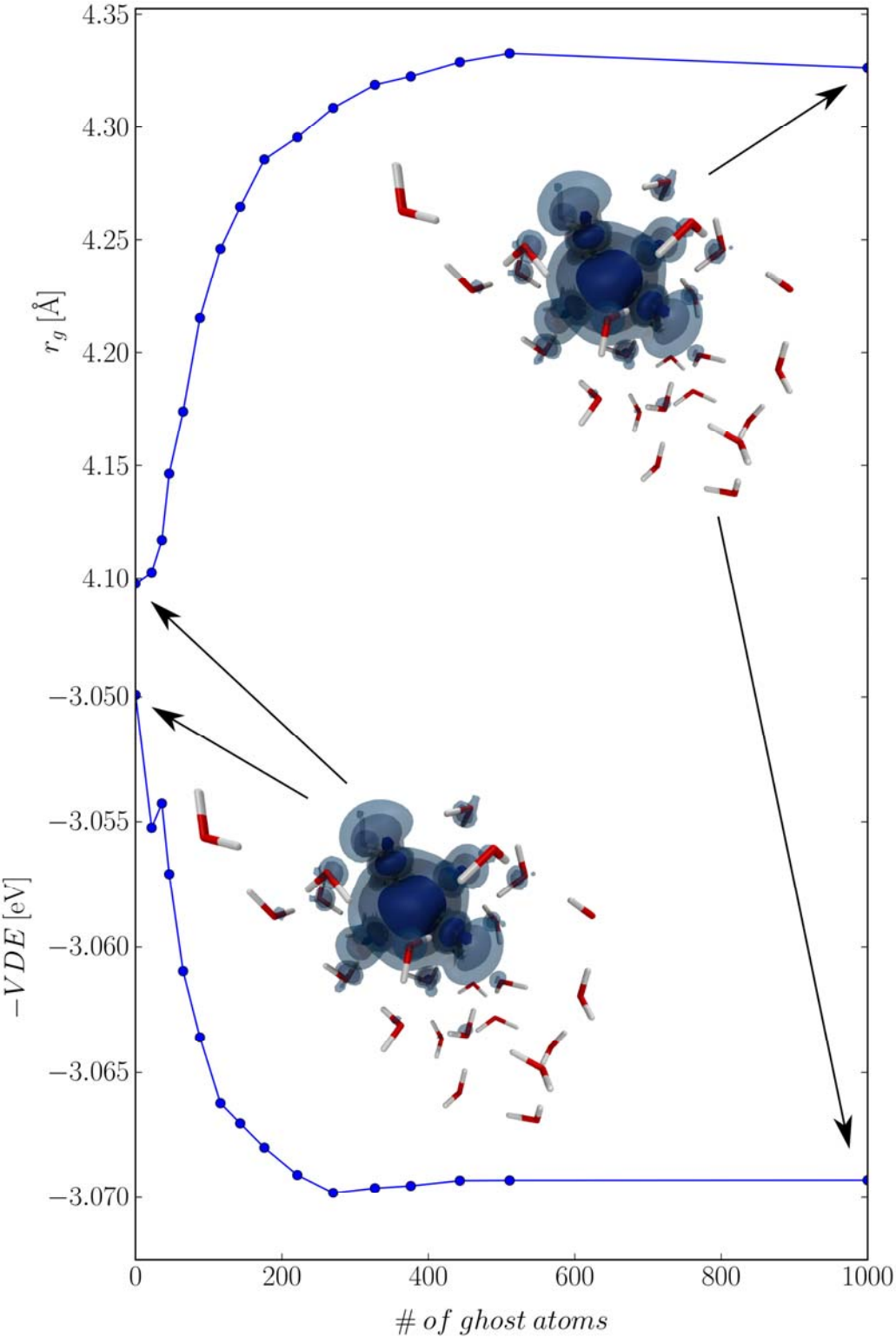
4.35
4.30
4.25
4.20
4.15
4.10
r_g [Å]
−3.050
−3.055
−3.060
−3.065
−3.070
$-VDE$ [eV]
0
200
400
600
800
1000
# of ghost atoms

Figure 10

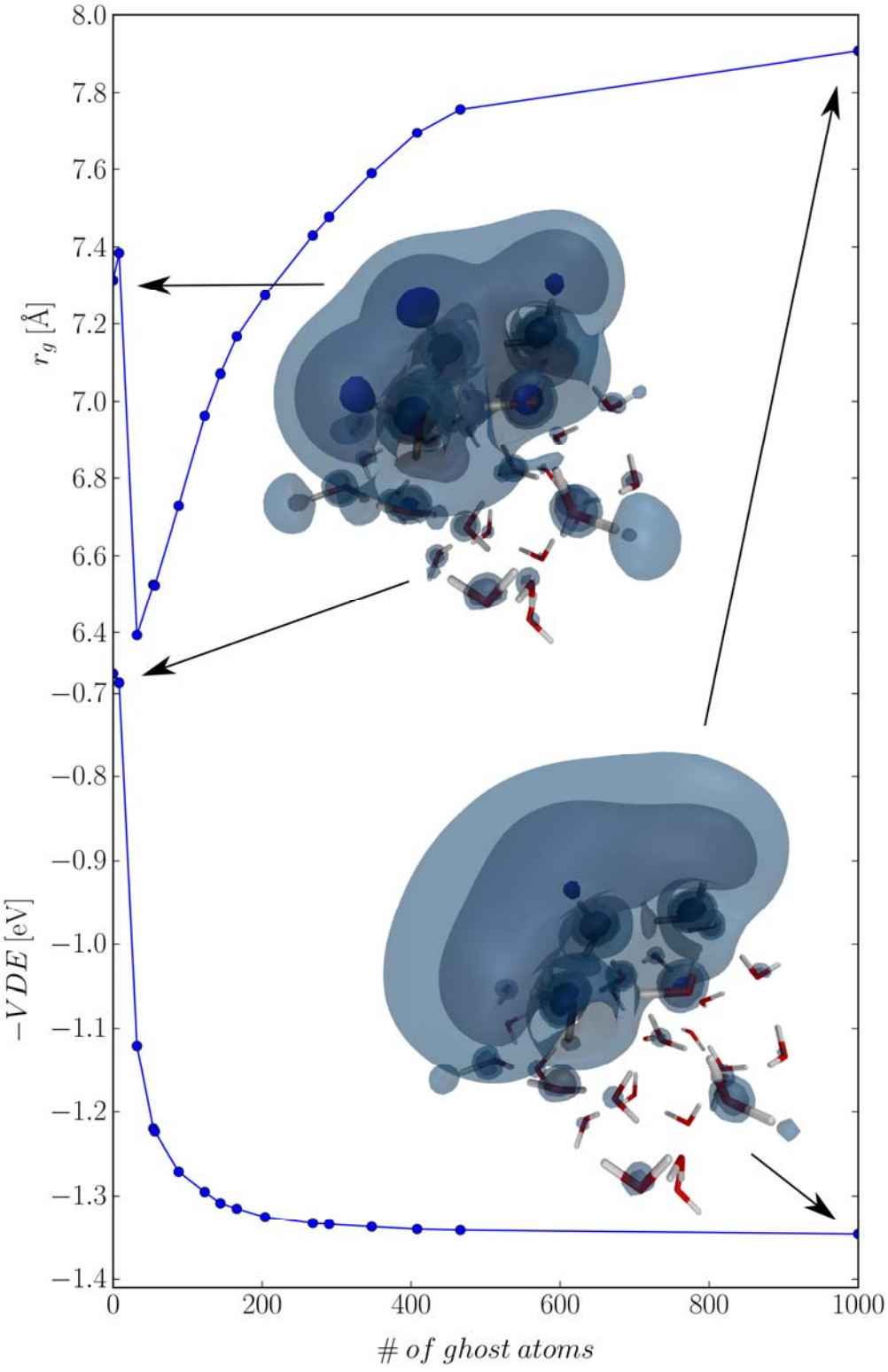
8.0
7.8
7.6
7.4
7.2
7.0
6.8
6.6
6.4
r_g [Å]
−0.7
−0.8
−0.9
−1.0
−1.1
−1.2
−1.3
−1.4
$-VDE$ [eV]
0
200
400
600
800
1000
# of ghost atoms

Figure 11

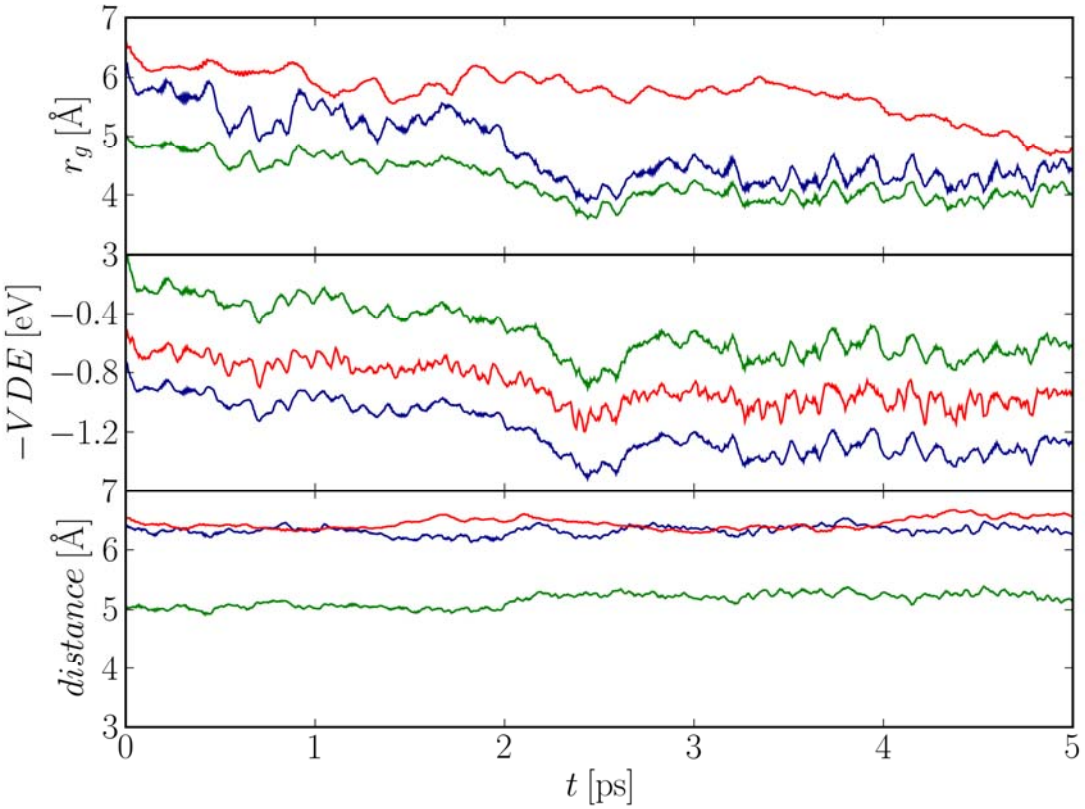

TOC: Excess electron localized on a cold water cluster.

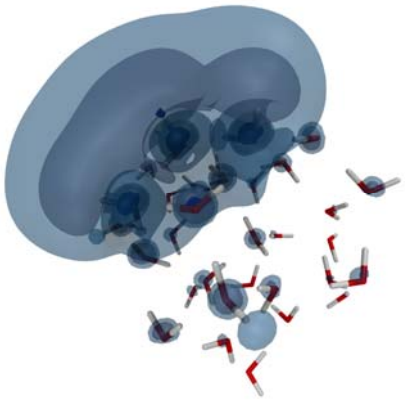

References

(1) Hart, E.; Anbar, M. *The hydrated electron*; Wiley-Interscience: New York, 1970.

(2) Crowell, R. A.; Bartels, D. M. *Journal of Physical Chemistry* **1996**, *100*, 17713.

(3) Vilchiz, V. H.; Kloepfer, J. A.; Germaine, A. C.; Lenchenkov, V. A.; Bradforth, S. E. *Journal of Physical Chemistry A* **2001**, *105*, 1711.

(4) Kambhampati, P.; Son, D. H.; Kee, T. W.; Barbara, P. F. *Journal of Physical Chemistry A* **2002**, *106*, 2374.

(5) Garrett, B. C.; Dixon, D. A.; Camaioni, D. M.; Chipman, D. M.; Johnson, M. A.; Jonah, C. D.; Kimmel, G. A.; Miller, J. H.; Rescigno, T. N.; Rossky, P. J.; Xantheas, S. S.; Colson, S. D.; Laufer, A. H.; Ray, D.; Barbara, P. F.; Bartels, D. M.; Becker, K. H.; Bowen, H.; Bradforth, S. E.; Carmichael, I.; Coe, J. V.; Corrales, L. R.; Cowin, J. P.; Dupuis, M.; Eisenthal, K. B.; Franz, J. A.; Gutowski, M. S.; Jordan, K. D.; Kay, B. D.; LaVerne, J. A.; Lymar, S. V.; Madey, T. E.; McCurdy, C. W.; Meisel, D.; Mukamel, S.; Nilsson, A. R.; Orlando, T. M.; Petrik, N. G.; Pimblott, S. M.; Rustad, J. R.; Schenter, G. K.; Singer, S. J.; Tokmakoff, A.; Wang, L. S.; Wittig, C.; Zwier, T. S. *Chemical Reviews* **2005**, *105*, 355.

(6) Coe, J. V.; Lee, G. H.; Eaton, J. G.; Arnold, S. T.; Sarkas, H. W.; Bowen, K. H.; Ludewigt, C.; Haberland, H.; Worsnop, D. R. *Journal of Chemical Physics* **1990**, *92*, 3980.

(7) Hammer, N. I.; Shin, J. W.; Headrick, J. M.; Diken, E. G.; Roscioli, J. R.; Weddle, G. H.; Johnson, M. A. *Science* **2004**, *306*, 675.

(8) Verlet, J. R. R.; Bragg, A. E.; Kammrath, A.; Cheshnovsky, O.; Neumark, D. M. *Science* **2005**, *307*, 93.

(9) Coe, J. V.; Arnold, S. T.; Eaton, J. G.; Lee, G. H.; Bowen, K. H. *Journal of Chemical Physics* **2006**, *125*.

(10) Coe, J. V.; Williams, S. M.; Bowen, K. H. *International Reviews in Physical Chemistry* **2008**, *27*, 27.

(11) Ehrler, O. T.; Neumark, D. M. *Accounts of Chemical Research* **2009**, *42*, 769.

(12) Ma, L.; Majer, K.; Chirot, F.; von Issendorff, B. *Journal of Chemical Physics* **2009**, *131*.

(13) Siefermann, K. R.; Liu, Y. X.; Lugovoy, E.; Link, O.; Faubel, M.; Buck, U.; Winter, B.; Abel, B. *Nature Chemistry* **2010**, *2*, 274.

(14) Neumark, D. M. *Nature Chemistry* **2010**, *2*, 247.

(15) Tang, Y.; Shen, H.; Sekiguchi, K.; Kurahashi, N.; Mizuno, T.; Suzuki, Y. I.; Suzuki, T. *Physical Chemistry Chemical Physics* **2010**, *12*, 3653.

(16) Roscioli, J. R.; Hammer, N. I.; Johnson, M. A. *Journal of Physical Chemistry A* **2006**, *110*, 7517.

(17) Turi, L.; Sheu, W. S.; Rossky, P. J. *Science* **2005**, *309*, 914.

(18) Frigato, T.; VandeVondele, J.; Schmidt, B.; Schutte, C.; Jungwirth, P. *Journal of Physical Chemistry A* **2008**, *112*, 6125.

(19) Madarasz, A.; Rossky, P. J.; Turi, L. *Journal of Chemical Physics* **2009**, *130*.

(20) Madarasz, A.; Rossky, P. J.; Turi, L. *Journal of Physical Chemistry A* **2010**, *114*, 2331.

(21) Marsalek, O.; Uhlig, F.; Frigato, T.; Schmidt, B.; Jungwirth, P., *submitted*.

(22) Becke, A. D. *Physical Review A* **1988**, *38*, 3098.

(23) Lee, C. T.; Yang, W. T.; Parr, R. G. *Physical Review B* **1988**, *37*, 785.

(24) Grimme, S. *Journal of Computational Chemistry* **2006**, *27*, 1787.

(25) Schmidt, J.; VandeVondele, J.; Kuo, I. F. W.; Sebastiani, D.; Siepmann, J. I.; Hutter, J.; Mundy, C. J. *Journal of Physical Chemistry B* **2009**, *113*, 11959.

(26) VandeVondele, J.; Sprik, M. *Physical Chemistry Chemical Physics* **2005**, *7*, 1363.

(27) Marsalek, O.; Frigato, T.; VandeVondele, J.; Bradforth, S. E.; Schmidt, B.; Schutte, C.; Jungwirth, P. *Journal of Physical Chemistry B* **2010**, *114*, 915.

(28) VandeVondele, J.; Hutter, J. *Journal of Chemical Physics* **2007**, *127*, 114105.

(29) Goedecker, S.; Teter, M.; Hutter, J. *Physical Review B* **1996**, *54*, 1703.

(30) Genovese, L.; Deutsch, T.; Neelov, A.; Goedecker, S.; Beylkin, G. *Journal of Chemical Physics* **2006**, *125*, 074105.

(31) VandeVondele, J.; Krack, M.; Mohamed, F.; Parrinello, M.; Chassaing, T.; Hutter, J. *Computer Physics Communications* **2005**, *167*, 103.

(32) Theodorou, D. N.; Suter, U. W. *Macromolecules* **1985**, *18*, 1206.

(33) Kim, S. K.; Park, I.; Lee, S.; Cho, K.; Lee, J. Y.; Kim, J.; Joannopoulos, J. D. *Physical Review Letters* **1996**, *76*, 956.

(34) Sommerfeld, T.; DeFusco, A.; Jordan, K. D. *Journal of Physical Chemistry A* **2008**, *112*, 11021.